Biomaterials 31 (2010) 6142–6153

Contents lists available at ScienceDirect

Biomaterials

journal homepage: www.elsevier.com/locate/biomaterials

The promotion of human malignant melanoma growth by mesoporous silica nanoparticles through decreased reactive oxygen species

Xinglu Huang [a,d], Jie Zhuang [b,d], Xu Teng [c], Linlin Li [a], Dong Chen [a], Xiyun Yan [b], Fangqiong Tang [a,*]

[a] Laboratory of Controllable Preparation and Application of Nanomaterials, Technical Institute of Physics and Chemistry, Chinese Academy of Sciences, Beijing 100190, China
[b] National Laboratory of Biomacromolecules, and China–Japan Joint Laboratory of Structural Virology and Immunology, Institute of Biophysics, Chinese Academy of Sciences, Beijing 100101, China
[c] Department of Biochemistry and Molecular, School of Basic Medical Sciences, Capital Medical University, Beijing 100069, China
[d] Graduate School of the Chinese Academy of Sciences, Beijing 100049, China

ARTICLE INFO

Article history:
Received 6 February 2010
Accepted 27 April 2010
Available online 26 May 2010

Keywords:
Mesoporous silica nanoparticles
Promotion tumor growth
Reactive oxygen species
Molecular mechanism

ABSTRACT

The concept that mesoporous silica nanoparticles (MSNs) are regarded as ideal novel drug delivery carriers in tumor therapy has been introduced extensively, but the effects of MSNs on tumor growth have received little attention. Here a model of nude mice xenografted with human malignant melanoma cells (A375) was used to investigate the effect of MSNs on tumor growth. Surprisingly, we found that MSNs have no toxicity to human malignant melanoma but increasing tumor growth *in vivo*. It was also confirmed that MSNs significantly promoted A375 cell proliferation and accelerated cell cycle progression *in vitro*. Cellular uptake mechanism showed that MSNs may affect molecular behavior of A375 cells when they entered into cytoplasm. Then, a detailed mechanism indicated that the promotion effect induced by MSNs was due to the decreasing of endogenous reactive oxygen species (ROS) in cells. Further results demonstrated that the upregulation of anti-apoptotic molecules Bcl-2 expression and the inhibition of NF-κB activation by MSNs may promote cell proliferation in a redox-sensitive signal pathway. These results show that tumor growth can be regulated by nanocarriers themselves in a ROS-dependent manner and imply that nanocarriers are not necessarily suitable for all kinds of tumor therapy in development drug delivery system.

1. Introduction

Ideal nanocarriers for tumor therapy need to have not only good therapeutic effect but also excellent biosafety. For the latter, it should be concerned the toxicity of nanocarriers for normal tissue, in the meantime, the effect of nanocarriers on tumor tissue cannot be ignored. However, limited knowledge exists on the effect of nanocarriers on tuning tumor growth. Effect of nanocarriers on tumor growth requires a thorough understanding of the mechanisms induced by nanoparticles (NPs), especially the molecular mechanism. Oxidative stress and reactive oxygen species (ROS) generation were shown to be some of the key mechanisms in cellular defense after NPs uptake [1]. ROS such as hydroxyl radical (•OH), superoxide anion ($O_2^{\bullet-}$) and hydrogen peroxide (H_2O_2) are widely investigated as signaling mediators of both protection and destruction of cells. NPs could induce intracellular oxidative stress by disturbing the balance between the oxidant and antioxidant processes. Previous researches have indicated that some NPs could trigger the generation of ROS which result in inflammation and even cell death [2,3]. However, some antioxidant properties of NPs were shown to be capable of scavenging hydrogen peroxide or superoxide and further to demonstrate the protective effects on cells. For example, Zhang et al. have demonstrated that the apoferritin-encapsulated Pt nanoparticles can decrease the intracellular ROS level and thus improve the viability of the cells [4]. Huang et al. have also shown that superparamagnetic iron oxide nanoparticles can promote human mesenchymal stem cells proliferation and accelerate cell cycle progression due to diminish intracellular H_2O_2 through the intrinsic peroxidase-like activity of iron oxide nanoparticles [5]. Thus, the theme of NPs-induced ROS production and scavenging capability has become an established paradigm for NP biosafety.

Mesoporous silica nanoparticles (MSNs) as nanocarriers, with a high BET surface area, large pore volume, uniform porosity, stable aqueous dispersion, excellent biocompatibility and *in vivo* biodegradability [6], have recently gained attention in drug/gene/protein

* Corresponding author. Technical Institute of Physics and Chemistry, Chinese Academy of Sciences, No.2 Beiyitiao Zhongguancun, Beijing 100190, China. Tel./fax: +86 10 82543521.
E-mail address: tangfq@mail.ipc.ac.cn (F. Tang).

0142-9612/$ – see front matter © 2010 Elsevier Ltd. All rights reserved.
doi:10.1016/j.biomaterials.2010.04.055

delivery [7,8], biosignal probing [9], biomarking [10], and many other important bioapplications. Recently multifunctional NPs have been prepared by encapsulation of photosensitizers into MSNs for photodynamic therapy (PDT) [11]. In a PDT process, absorption of light will promote the photosensitizer molecules to initiate the generation of ROS in tumor cells. Some anticancer drug, such as camptothecin [12], can also be incorporated into the pores of MSNs and delivered into a variety of human cancer cells to induce cell death by ROS-dependent mechanism [13]. But few papers have reported whether MSNs also cause the changes of ROS level in cells by themselves.

Nuclear factor κB (NF-κB) and Bcl-2 involved in antioxidant pathway play important role in the regulation of cell apoptosis and cell survival. NF-κB is a ubiquitous nuclear transcription factor that plays a major regulatory role in the balance between cell survival and apoptosis via expression of its target genes [14]. The activation of NF-κB is dependent on degradation of IκB which is bound to p50/p65 in cytoplasm and thus forming an inactive trimeric complex, causing the release and translocation of the NF-κB complex into the nucleus. There has been increasing evidence supporting that the redox-sensitive NF-κB regulates the activity and/or expression of anti-oxidative and anti-apoptotic target genes and promotes cell survival against oxidative cell death [15]. Bcl-2 is a key molecule regulating cell apoptosis, a deliberate life-relinquishment of the cell. Bcl-2 prevents apoptosis caused by a variety of cellular stress such as oxidative stress, heat shock, and cytokine deprivation. Experimental data from *in vitro* and *in vivo* studies suggest that Bcl-2 may block apoptosis through regulation of cellular antioxidant defense mechanisms, which has been considered to act as a free radical scavenger [16]. Thus, ROS are the potent regulators of the NF-κB activation and Bcl-2 expression, but it is not entirely clear whether the changes of ROS induced by NPs regulated the activation of NF-κB and the expression of Bcl-2 and further affected cell cycle and cell proliferation.

In this study, we have studied the effect of MSNs on human malignant melanoma growth and demonstrated the signal transduction mechanism of human malignant melanoma (A375) cells induced by MSNs. First, the effects of MSNs on tumor growth *in vivo* and A375 cells proliferation *in vitro* were observed. Cellular uptake, uptake mechanism and intracellular fate of MSNs were researched to understand the interaction between MSNs and A375 cells. Next, the effect of MSNs on the endogenous reactive oxygen species (ROS) level of A375 was also investigated to explain the molecular mechanism of MSNs-promotion A375 cells growth. Finally, the NF-κB activation and Bcl-2 overexpression associated to ROS generation and cell proliferation were also investigated.

2. Materials and methods

2.1. Materials

Cetyltrimethylammonium bromide (CTAB), tetraethyl orthosilicate (TEOS), aqueous ammonia, 3-aminopropyltriethoxysilane (APTES), dimethylformamide (DMF), fluorescein isothiocyanate (FITC) and sucrose were obtained from Beijing Chemical Reagents Company (China). Dulbecco's modified Eagle's medium (DMEM) and fetal bovine serum (FBS) were from Gibco. Bovine serum albumin (BSA), Triton X-100, filipin, sodium azide (NaN_3), propidium iodide (PI) and 3-[4,5-dimethylthiazolyl-2]-2,5-diphenyltetrazolium bromide (MTT) were obtained from Sigma. LysoTracker Red, catalase analysis kit and colorimetric microplate assay kit were purchased from Beyotime Biotechnology Company (China). 4,6-diamidino-2-phenylindole (DAPI) and 2,7-Dichlorofluorescein diacetate (DCFH-DA) were from Invitrogen. Anti-NF-κB (p50), anti-NF-κB (p65), anti-IκB, anti-Bcl-2, anti-actin antibodies and horseradish peroxidase (HRP)-conjugated secondary antibodies were provided by Santa Cruz. Human melanoma cell lines (A375), human breast cancer cell lines (MDA-MB-231), human embryonic kidney 293 T cells (HEK293T), human microvascular endothelial cells (HMEC) were purchased from ATCC.

2.2. MSNs synthesis and characterization

MSNs were synthesized by condensation under diluted TEOS and low surfactant conditions with aqueous ammonia as a catalyst [17]. Briefly, 6 mM CTAB was dissolved in 70 ml H_2O, and 1.5 ml $NH_3 \cdot H_2O$ (28%–30%) was added with stirring. The stirring was continued for 1 h, and then 0.6 ml TEOS was added with vigorous stirring for 4 h at room temperature. The MSNs were collected by centrifuging at 12,000 rpm for 20 min and then washed and redispersed with ethanol and deionized water several times. The solid products were obtained by centrifugation and dried at 60 °C overnight. The surfactant templates were removed by gradient calcination for 5 h and MSNs were obtained. Morphology and mesostructure images were observed with a JEM 2100 transmission electron microscope (TEM).

2.3. Modification and fluorescent labeling of MSNs

Particle surfaces were functionalized by the addition of primary amines, using 3-aminopropyltriethoxysilane (APTES) to attach alkoxy silane groups to surface hydroxiles [9]. These amine groups were then available for the attachment of FITC molecules. 20 mg of the MSNs were dispersed in 20 ml of anhydrous DMF. A solution of 10 μl APTES diluted in 200 μl DMF was added to the particle suspensions, sonicated, and stirred at room temperature for 20 h. The modified MSNs were collected by centrifugation. After washing three times, the modified MSNs were resuspended in 3 ml of Tris–Cl buffer (pH 8.6). Then 100 μg/ml FITC were added. The suspension was stirred for 8 h, and the FITC-labeled MSNs (MSN-FITC) were collected by centrifugation. After thoroughly washing the labeled materials with Tris–Cl buffer, the particles were dried under vacuum and stored as dry powders. FITC-labeled MSNs were used only for the internalization studies.

2.4. Nude mice xenografted with A375 cells

0.2 mg/ml MSNs were added into A375 cells for 24 h prior to tumor initiation. Cells treated and untreated with MSNs were collected, concentrated by centrifugation, counted using a haemocytometer and resuspended in an appropriate volume of the conditioned growth medium. 10^7 A375 cells in 200 μl of growth media were injected subcutaneous onto the flanks of 6–8 week old Balb/c athymic nude mice. In order to distinguish between individual differences in mice, six mice were chosen and the A375 cells untreated with MSNs were injected subcutaneous onto their left flank and the cells cultured in the presence of MSNs were injected onto their right flank. The promotion effect of tumor growth was evaluated in terms of tumor volume (mm^3). Tumor dimensions were determined at various time points using a caliper. Tumor volume (mm^3) was calculated using the following formula [18]: Tumor volume (mm^3) $= a \times b^2/2$, where a is the length and b is the width in millimeters.

2.5. Cell proliferation assays

The cytotoxicity of MSNs was evaluated by MTT viability assays. A375 cells were grown routinely in DMEM supplemented with 10% FBS and were maintained in a humidified incubator. For cytotoxicity assays, A375 cells were cultured (8000 cells per well) on 96-well plates for different time with different concentrations of MSNs treatment. A375 cells cultured in the absence of MSNs acted as controls. The viability of A375 cells was determined using a MTT proliferation assay kit. Briefly, 10 μl MTT reagent was added to each well and incubated for 4 h until a purple precipitate was visible. 100 μl 10% SDS was then added to each well and left in the dark at room temperature for 24 h. The absorbance of the resulting formazan solution was recorded at 590 nm with a microplate reader (Bio-Rad, USA).

2.6. Cell cycle analysis

MSNs treated and untreated A375 cells (1×10^6) were fixed using a solution containing 70% ethanol in PBS for 12 h at 4 °C. The cells were then centrifuged at 1500 rpm for 10 min to remove the fixation solution. The cell pellets were incubated with DNA staining solution (40 μg/ml PI and 100 μg/ml RNase A in PBS) for 30 min in the dark. Ten thousand cells per sample were analyzed using flow cytometry.

2.7. Cellular uptake, uptake mechanism and intracellular fate studies

2.7.1. Cellular uptake studies

For confocal microscopy, A375 cells were plated 24 h before the start of the experiment in chamber slides at a density of 5×10^3 cell/cm^2. After incubation with 50 μg/ml MSN-FITC for 4 h, the A375 cells were then washed twice with PBS and incubated with 0.1% Triton X-100 plus 1% BSA in PBS at room temperature for 15 min followed by 5 μg/ml DAPI staining in PBS for 30 s at room temperature. The slides were washed twice with PBS and then examined with a confocal laser scanning microscope (Olympus, Tokyo, Japan).

2.7.2. Uptake mechanism studies

To understand the uptake mechanism of MSNs, cells were treated as previous described method [19]. Experiments Blocking the Endocytosis (Energy-Dependent Process): For low temperature incubation, the cell was cultured at 4 °C instead of 37 °C. For the incubation with MSNs-FITC under ATP depletion, the cells were pre-incubated in PBS buffer, supplemented with NaN_3 (10 mM) during 30 min at 37 °C, and then 50 μg/ml MSNs-FITC were added.

Hypertonic Treatment to Hinder the Clathrin-Mediated pathway: The cells were pre-incubated for 30 min in PBS buffer supplemented with sucrose (0.45 M) at 37 °C, and then 50 μg/ml MSNs-FITC were added.

Filipin Treatment Blocking Caveolae Pathway: The cells were pretreated in PBS buffer and supplemented with filipin (5 μg/ml) for 30 min followed by incubation with 50 μg/ml MSNs-FITC at 37 °C.

The above treated A375 cells were washed three times with PBS, and then harvested by trypsinization. After centrifuging, the cell pellet was washed once and resuspended with PBS containing 0.1% FBS. The cellular uptake of MSN-FITC was quantitatively determined by fluoresceneactivated cell sorting (FACS) (Becton Dickenson, Mississauga, CA).

2.7.3. Intracellular fate of MSNs

A375 cells were treated with LysoTracker Red (50 nM) for 1 h at 37 °C following the supplier's protocol, and then with MSNs-FITC (50 μg/ml) for an additional 4 h. The cells were rapidly washed with ice cold PBS to prevent the removal of the attached LysoTracker Red, fixed, and prepared for visualization a confocal microscope.

2.8. Measurement of hydrogen peroxide

Hydrogen peroxide production was measured using DCFH-DA assay as described previously [20]. In briefly, the A375 cells treated with or without MSNs were washed with DMEM medium and were incubated in the dark with DCFH-DA (5 μM) for 15 min at 37 °C. The cells were harvested, washed once, and resuspended in PBS. Fluorescence was monitored using a FACS. The mean of DCF fluorescence intensity was obtained from 10,000 cells using 480 nm excitation and 540 nm emission settings. By using the same settings, the fluorescent intensity was obtained from each experimental group.

For confocal microscopy, the A375 cells were plated 24 h before the experiment. After incubation with the concentration of 0.2 mg/ml MSNs for different time or with different concentration MSNs for 1 h, the A375 cells were then washed twice with PBS and were incubated in the dark with DCFH-DA (5 μM) for 15 min at 37 °C. The slides were washed twice with PBS and then examined by a confocal microscope.

2.9. Analysis of oxidant scavengers

2.9.1. Semiquantitative reverse transcription-PCR

Total RNA was extracted from the A375 cells by using the RNeasy Mini Kit (Qiagen Inc, Valencia, CA) according to the manufacturer's recommendations. First-strand cDNAs were synthesized using total RNAs, reverse transcriptase, and an oligo (dT) primer (Roche, USA). Primers used for PCR amplification were as follows: NADPH oxidase 4 (NOX4) forward: 5′-CTGGAGGAGCTGGCTCGCCAACGAAG-3′ and reverse: 5′- GTGATCATGAGGAATAGCACCACCACCATGCAG-3′; Catalase forward: 5′-TCCATTCGATCT CACCAAGG-3′ and reverse: 5′-GTAGTAATTTGGAGCACCACC-3′; Cu/Zn SOD forward: 5′-TGAAGAGAGGCATGTTGGAG-3′ and reverse: 5′-TCTTCATTTC-CACCTTTGCC-3′; Mn SOD forward: 5′-GACAAACCTCAGCCCTAAC-3′ and reverse: 5′-TGCTCCCACACATCAATCC-3′. GAPDH forward: 5′-ACCACCATGGAGAAGGCTGG-3′ and reserve 5′-CTCAGTGTAGCCCAGGATGC-3′. The final PCR mixture contained 1 μl cDNA template and 400 nM of the forward and reverse primers in a final volume of 20 μl. Samples were run concurrently with a standard curve prepared from the PCR products. PCR conditions were three 3 min steps of 94 °C and 40 cycles of 94 °C for 15 s, 55 °C for 30 s, and 72 °C for 30 s. Quantification of PCR product was done by electrophoresis. For semi-quantization amounts of RNA were estimated by the relative intensity against the relative intensity of GAPDH.

2.9.2. Catalase activity

The A375 cells were treated with or without NPs at a concentration of 0.2 mg/ml for 12 h. The culture medium and cell extract were collected for measurements of human catalase activity by a catalase analysis kit as described previously [21]. Briefly, samples were treated with excess hydrogen peroxide for decomposition by catalase for an exact time, and the remaining hydrogen peroxide coupled with a substrate was treated with peroxidase to generate a red product, N-4-antipyryl-3-chloro-5-sulfonate-p-benzoquinonemonoimine, which absorbs maximally at 520 nm. Catalase activity was thus determined by measuring the decomposition of hydrogen peroxide spectrophotometrically. The protein concentration was measured with a Bradford protein assay kit.

2.9.3. GSH and GSSG

Total glutathione (GSH) and oxidative glutathione (GSSG) levels were measured by the colorimetric microplate assay kits as described previously [22]. Briefly, 40 μl metaphosphoric acid was added into 10 μl sub-brain homogenates and then centrifuged for 10 min. The supernatant was used for GSH and GSSG assay. The total GSH level was measured by the method of DTNB-GSSG recycling assay. The GSSG level was quantified by the same method of total GSH assay after the supernatant was pretreated with 1% 1 M 2-vinylpyridine solution to remove the reduced GSH. The amount of reduced GSH was obtained by subtracting the amount of GSSG from that of the total GSH.

2.10. Confocal immunofluorescence microscopy and western blot

A375 cells were plated on coverslips and cultured in a culture dish overnight. After stimulation with MSNs for 12 h with different concentration, the cells were washed with PBS, fixed in 4% cold polyformaldehyde (PFA) in PBS for 10 min, and then permeabilized with 0.1% Triton X-100. After washing with PBS, the cells were blocked in 5% normal goat serum for 30 min, and then incubated with primary antibodies at 37 °C for 1 h. The A375 cells were then washed with PBS and PBST and incubated with secondary antibody at 37 °C for 30 min. Finally, the coverslips were examined with a confocal microscope.

Total cellular protein extracts were prepared in radioimmunoprecipitation assay buffer (RIPA) and were transferred to Hybond membranes after separation by 10% SDS-PAGE. The membranes were blocked with 5% milk in PBS for 1 h, incubated for 2 h with primary antibodies, and then probed for 1 h with HRP-conjugated anti-mouse or anti-rabbit IgG. After extensive washing with PBST, the target proteins were detected on the membranes by enhanced chemiluminescence.

2.11. Statistical analysis

The level of significance in all statistical analyses was set at a probability of $p < 0.05$. Data are presented as means ± SD. Analysis of variance and *t* tests was used to analyze the data.

3. Results

3.1. Synthesis and characterization of well-ordered monodisperse mesoporous silica nanoparticles (MSNs)

MSNs with well-ordered hexagonal pore structures were synthesized under dilute tetraethyl orthosilicate (TEOS) and low surfactant concentration conditions with aqueous ammonia as a catalyst. The TEM image showed that the as-synthesized MSNs were composed of large numbers of discrete worm-like pores (Fig. 1A). The overall average diameter of MSNs was 110 nm with 14% polydispersity. The XRD patterns exhibited up to three hexagonal characteristic reflection peaks (100), (110) and (200) indicating highly ordered mesostructure within MSNs (Fig. 1B). The pore properties and surface area of the MSNs were further analyzed by N_2 adsorption–desorption isotherms (Fig. 1C). The products possess high BET surface area (1169 $m^2 g^{-1}$) and the average pore size of MSNs was 2.4 nm. These results indicated that the MSNs were potential bio-carriers with therapeutic or diagnostic gene/drug for developing delivery systems. In addition, we also measured the ζ potential of APTES modified MSNs as described in Section 2.3. After the modification of MSNs, the ζ potential of different derivated MSNs varied from −35.6 mV (unmodified) to 27.5 mV (amino group modified). The change of the ζ potential indicated that the MSNs were modified successfully which were suitable for the conjugation of FITC.

3.2. MSNs promote human malignant melanoma growth

To investigate the effect of MSNs on human malignant melanoma growth, A375 cells untreated or treated by MSNs were injected subcutaneous to both flanks of six Balb/c athymic nude mice to initiate tumor: left flank was the A375 cells untreated with MSNs and right flank was the MSNs treated cells. In contrast to the untreated, the larger tumor volume in MSNs treated A375 cells bearing mice was observed after tumor xenografts for 20 days (Fig. 2A). When the tumors were dissected from mice, a clear promotion tumor growth effect was seen after MSNs treatment (Fig. 2B). To study the detailed information of tumor growth over time, tumor volumes were measured at a time interval. As Fig. 2C shown, there was a more rapid rate of tumor growth than control, which indicating the promotion effect of MSNs on human malignant melanoma growth. These results suggested that MSNs themselves improved human malignant melanoma growth *in vivo*.

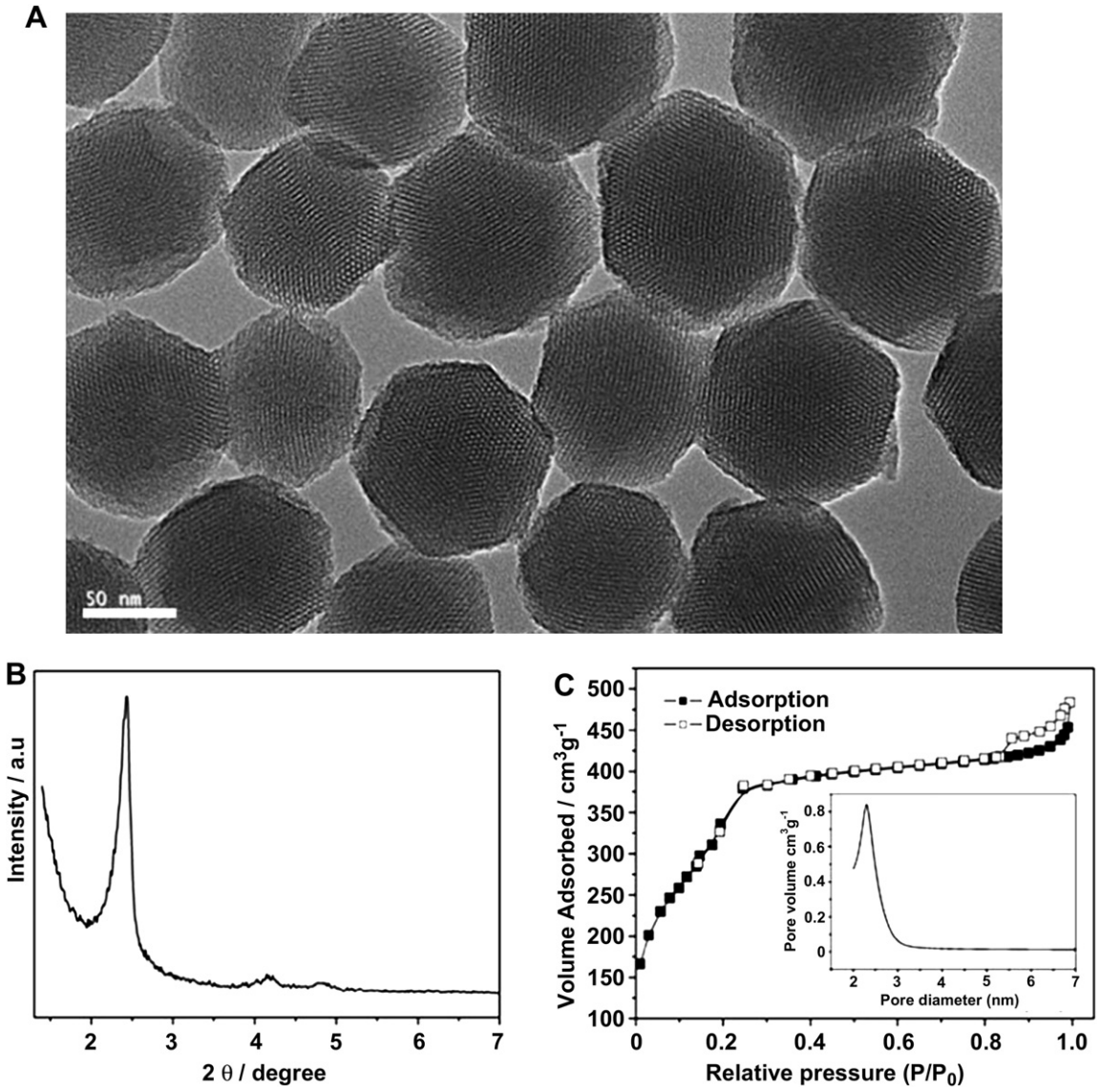

Fig. 1. Characterization of MSNs. (A) Transmission electron microscopy (TEM) images; (B) XRD pattern of MSNs; and (C) N_2 adsorption/desorption isotherms and mesoporous distribution curve.

3.3. *Effect of monodisperse MSNs on cell proliferation and cell cycle*

To find the reasons for the promotion of human malignant melanoma growth, the effect of MSNs on cell proliferation of A375 cells was studied. After treated with different concentrations (0.0625, 0,125, 0.25 and 0.5 mg/ml) of MSNs for 24 h or with the same concentrations of MSNs for different times (6, 18, 24, 30, 42 h), the cell proliferation was analyzed by MTT assays, respectively. As shown in Fig. 3A and B, MSNs promoted A375 cells proliferation in both concentration- and time-dependent manner. The viability of A375 cells was clearly increased with the concentration decreasing and the time increasing compared to the control group ($p < 0.01$). To study the effect of MSNs on cell proliferation of other cell lines, additional three kinds of cell lines were chosen including human normal (HEK293T and HMEC) cells and tumor (MDA-MB-231) cells. Cell viability of these three kinds of cells (HEK293T, HMEC and MDA-MB-231) was evidently not altered in both a concentration- and time-dependent manner (Supplemental Fig. 1). These results indicated that MSNs specifically promoted cell proliferation of A375 cells which were in a cell type dependent manner.

Different NPs are known to have the effects on genes controlled cell cycle progression and induction of pro- or anti-apoptotic genes expression. NPs promote cell growth and proliferation primarily through its effect on the cell cycle or induction of apoptosis. Subsequently, the effects of MSNs on the percentages of cell cycle phases (G1, S, and G2/M) were quantified by FACS. As shown in Fig. 3C, after treatment with MSNs for 24 h, a significant increase in S and G2/M phases was observed. Cells treated with MSNs had a higher proportion of S (28.29%) and G2/M phase (6.62%) as compared to the control which had a proportion of 17.14% and 5.43%, respectively. Thus, the promoting proliferation property of MSNs could be attributed to increasing cell cycle progression.

3.4. *MSNs specifically promoted cell proliferation due to decrease ROS level*

In previous reports, ROS generation and oxidative stress measurement have been developed to evaluate cytotoxicity of NPs. The changes of ROS generation strongly influenced cell proliferation and caused apoptosis in cells incubated with NPs [23]. It has

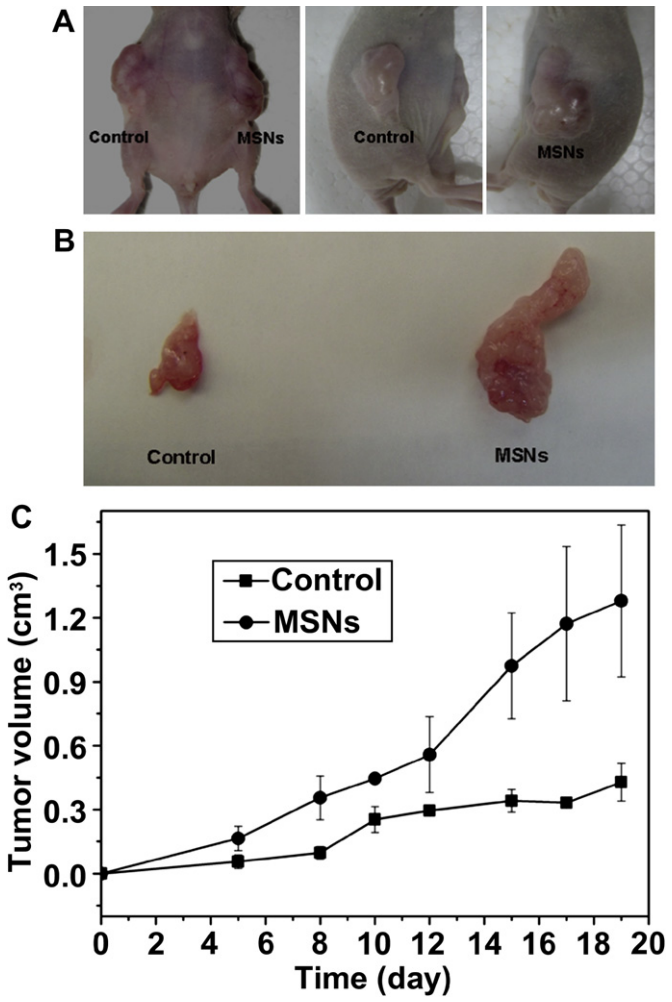

Fig. 2. MSNs promotes melanoma tumor growth in A375 xenografted mice. (A) Images of tumor in both flanks of mice: left flank is untreated with MSNs (middle) and right flank is treated with MSNs (right). (B) Images of tumor after dissection from mice. (C) Promotion tumor growth was assessed by tumor volume.

been reported that some NPs-promoted cell growth was due to its ability to diminish intracellular H_2O_2 [4,5]. Thus, we hypothesized the cell proliferation induced by MSNs was caused by the diminishing of intracellular ROS level. To verify the hypothesis, ROS level of A375 cells treated with MSNs was detected using dichlorofluorescein diacetate (DCFH-DA), a ROS fluorescent dye. In the presence of H_2O_2 or hydroxyl ($OH\cdot$) radicals, DCFH was oxidatively modified into a highly fluorescent derivative, 2,7-dichlorofluorescein (DCF). DCF fluorescence was detected in A375 cells by fluorescent imaging and FACS. Visualization of ROS level with confocal microscope showed that oxidized DCF fluorescence was significantly decreased in the cell cultured in the presence of MSNs (0.2 mg/ml) compared to the untreated group (Fig. 4A and B). This means that endogenous ROS of cells was diminished in response to the treatment with MSNs. To better determine the ROS scavenging capability of MSNs, the fluorescence intensity of A375 cells was measured using FACS (Supplemental Fig. 2A). The ROS level of A375 cells was decreased in a concentration- and time-dependent manner as shown in Fig. 4C and D. After A375 cells incubated with 0.2 mg/ml MSNs for 1 h at least, a more than twice decrease of the ROS level in cells was observed. However, treatment of HMEC, HEK293T and MDA-MB-231 cells with MSNs was not changed ROS generation (Supplemental Fig. 2B–D). Together with Section 3.3 and the previous report [5], it could be concluded that the increase of cell proliferation may be attributed to the decrease of endogenous ROS level.

3.5. Cellular uptake, internalization mechanism and intracellular fate of MSNs

To investigate cellular internalization of the particles, the MSNs were first modified by APTES for covalent conjugation with FITC as described in Section 2.3. MSNs labeled FITC (MSNs-FITC) were then incubated with A375 cells for 4 h. Merged confocal microscope images of A375 cells (Fig. 5A–D) showed that MSNs-FITC were internalized into the cells. Inside the A375 cells, MSN-FITC formed nonuniform green fluorescent aggregates and accumulated in the perinuclear region. It was not observed the green fluorescence in the nucleus, whose reason was that the size of MSNs was too large to penetrate the nuclear pore of cells.

In an effort to identify the internalization mechanism of MSNs, the A375 cells were previously incubated with endocytosis inhibitors, such as NaN_3, sucrose and filipin, and then were incubated with 50 μg/ml MSNs-FITC. Cells incubation at 4 °C is also known to block endocytosis. The NaN_3 treatment disturbs the production of ATP and blocks the energy-dependent endocytic pathway. The receptor-mediated endocytic pathway is inhibited after pretreatment with sucrose or filipin: sucrose inhibits the formation of clathrin-mediated pathway; filipin inhibits caveolae pathway. After incubated at 4 °C, the amount of MSNs-FITC uptake by A375 cells was analyzed by FACS which indicating the MSNs-FITC uptake was entirely inhibited (Fig. 5E and F). However, the inhibitory effect of NaN_3 on MSNs-FITC uptake was not observed. When A375 cells were pre-incubated with sucrose and then treated with MSNs-FITC, the uptake of MSNs-FITC was reduced by 80% compared to the cells did not treat with sucrose. In contrast to the clathrin pathway blocking experiment, we observed that pretreatment with filipin did not hinder the internalization of MSNs-FITC. These results indicated that MSNs were mainly internalized by cells by the clathrin-mediated pathway.

In order to track the MSNs following their uptake, the lysosomal compartment of A375 cells was stained with the LysoTracker Red probes, and then the cells were treated with MSNs-FITC. Cell nucleus was labeled with DAPI staining (blue color). The colocalization of MSNs-FITC with lysosome produced a yellow fluorescence in merged images. As Fig. 5J shown, some aggregates of MSNs were found entrapped in the lysosomal vesicles. Some MSNs-FITC were dispersed into the cytosol and accumulated in the perinuclear region of cells (arrow), which indicated that MSNs escaped from lysosomal entrapment and then entered the cytoplasm.

3.6. Effect of MSNs on the expression/activity of redox system components

In order to examine the effect of the MSNs on the activity of antioxidant enzymes, catalase (CAT) activity was measured in the cell culture medium and cell lysates with or without the treatment of MSNs at a concentration of 0.2 mg/ml for 12 h. The CAT activity was no marked change in the culture medium after treatment with MSNs, while the CAT activity in cell lysates was significantly increased (Fig. 6C). To further confirm the expression increase of CAT in A375 cells, mRNA expression of CAT was quantified by RT-PCR and indicated that the expression of CAT was obviously upregulated ($p < 0.01$) with the treatment of MSNs (Fig. 6A and B). CAT is a potent scavenger of H_2O_2 and can protect cell or tissues from damage by consuming H_2O_2. The production of CAT provides antioxidative activity against oxidative stress, thus, the expression increase of CAT was one of the important factors for ROS decrease in A375 cells.

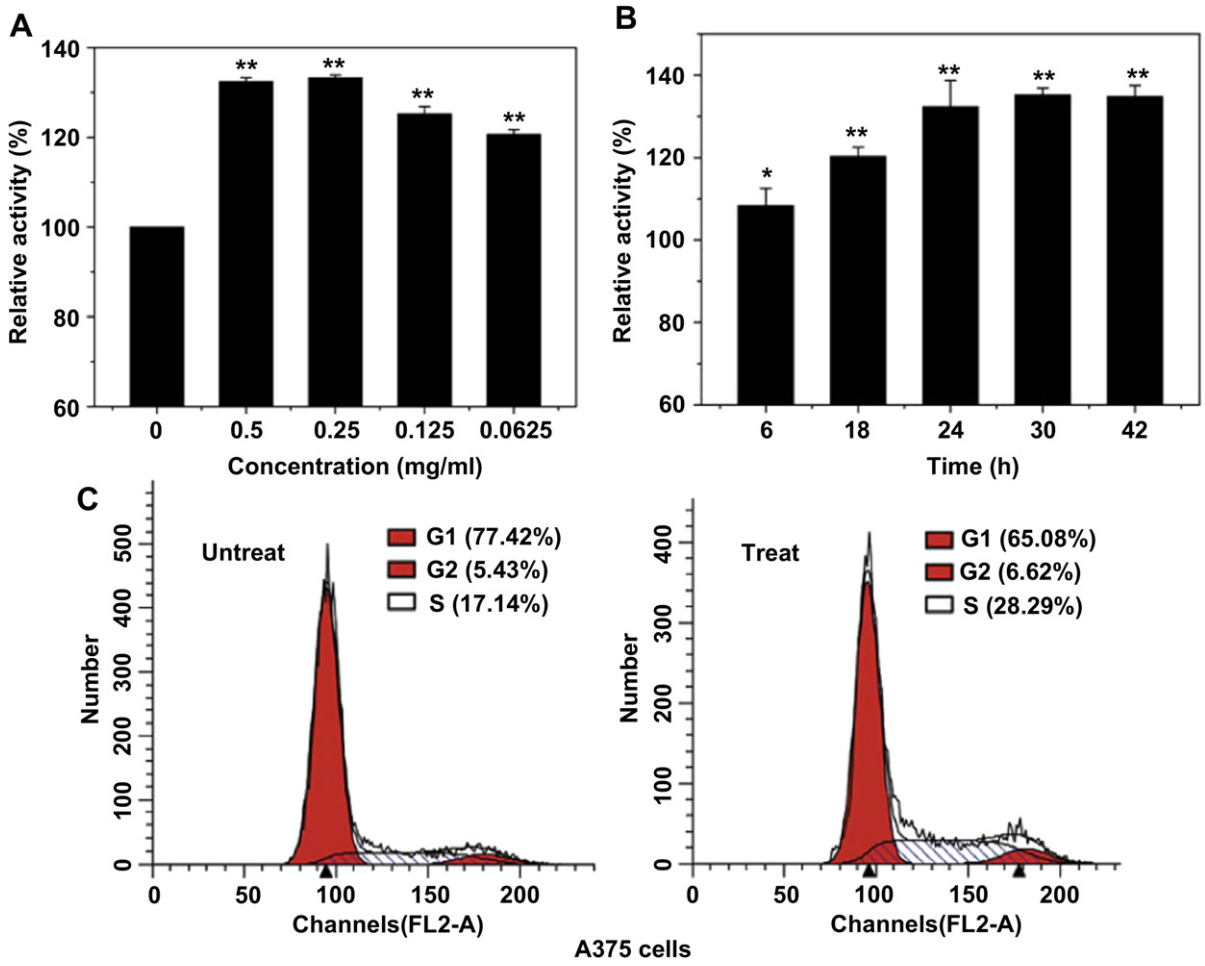

Fig. 3. Effect of MSNs on A375 cell proliferation and cell cycle. Effect of MSNs on cell proliferation (A) after the incubation for 24 h with different concentration of particles, and (B) after the incubation for different time with 0.2 mg/ml particles. (C) Analysis of MSNs on cell cycle progression using FACS after treatment with 0.2 mg/ml MSNs for 24 h. (Data are means ± SD from three separate experiments. ** denotes statistical significance for the comparison of cell proliferation treatment with or without MSNs, $p < 0.01$).

GSH is the most abundant thiol species in cell cytoplasm, functioning as a natural oxidant scavenger and the major reducing agent in biochemical processes. Its oxidized form is glutathione disulfide (GSSG). The antioxidant action of GSH is due to the redox reaction that readily occurs between GSH and GSSG. To investigate the influence of MSNs on cellular ROS level, the intracellular GSH and GSSG level was determined. A375 cells treated with MSNs were found to have an increase level of GSH, comparing with untreated cells (Table 1). Correspondingly, a three fold decrease of GSSG level in cells was observed ($p < 0.05$). Analysis of GSH/GSSG ratio revealed that the GSH/GSSG in treated cells were significantly increased four times ($p < 0.01$). From above results, it could be found that the decrease of endogenous ROS was relative to the increase of intracellular GSH.

The NADPH oxidase (NOX) family of superoxide ($O_2^{\cdot-}$) and hydrogen peroxide (H_2O_2)-producing proteins has emerged as an important source of ROS in signal transduction. In terms of structural basis, the NOX enzymes are classified into three distinct groups: NOX1-4, NOX5, and Duox. With regard to A375 cells, mRNA expression of NOX 1-5 was quantified by RT-PCR and indicated that only NOX4 was presence (data not shown). NOX4 tissue distribution has considered as fairly ubiquitous, and in general NOX4 is highly expressed compared to other NOX homologues [24]. The mRNA expression of NOX4 was evidently down-regulated ($p < 0.01$) with the treatment of MSNs compared to the control (Fig. 6A and B). These results indicated that NOX4 played important role in the change of endogenous ROS.

SOD, which catalyzes the dismutation of the superoxide anion into hydrogen peroxide and molecular oxygen, is one of the most important antioxidative enzymes and plays an important role in the balance between oxidation and antioxidation of the organism. Three distinct isoforms of SOD have been identified and characterized in mammals [25]: copper–zinc superoxide dismutase (Cu/Zn SOD; encoded by the *sod1* gene), manganese superoxide dismutase (Mn SOD; encoded by the *sod2* gene), and extracellular superoxide dismutase (EC SOD; encoded by the *sod3* gene). The mRNA expression of Cu/Zn SOD in A375 cells was found to increase distinctly after treatment with MSNs at a concentration of 0.2 mg/ml for 12 h ($p < 0.05$), corresponding to 134% of control (Fig. 6A and B). Similarly, the mRNA expression of Mn SOD was clearly increased when compared with the controls ($p < 0.05$). These results indicated that SOD also played important role in decreasing ROS of A375 cells.

3.7. NF-κB and Bcl-2 signal transduction were involved in MSNs induction of ROS decrease

Based on the report that the transcription factor NF-κB played a pivotal role in the development of cell survival and proliferation and was known to be responsive to oxidative stress [26], we

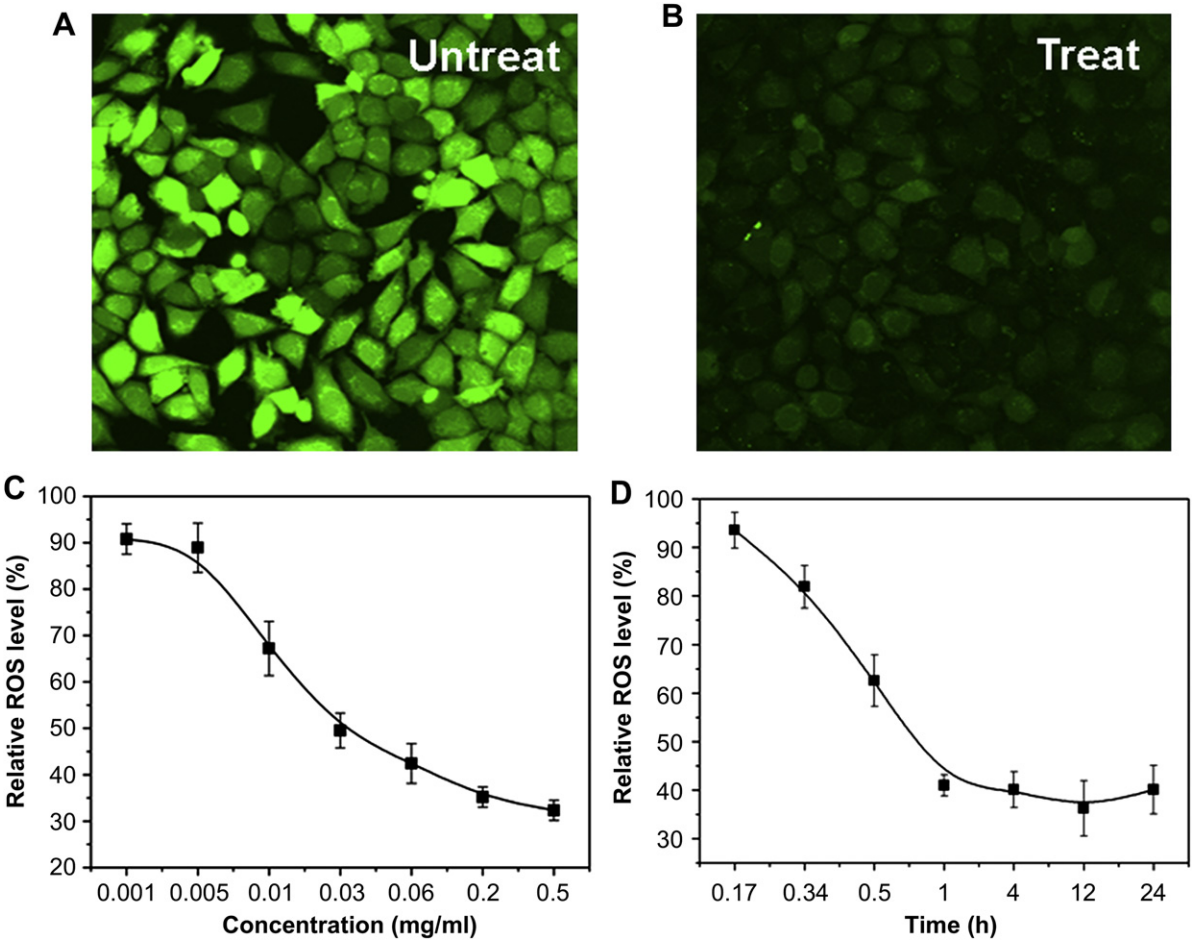

Fig. 4. Effect of MSNs on endogenous reactive oxygen species (ROS) level in A375 cells. (A, B) Confocal microscopy images of ROS in A375 cells after the incubation for with MSNs for 24 h. (C, D) Effect of MSNs on ROS generation in A375 cells (C) with different concentration MSNs treatment for 1 h or (D) with 0.2 mg/ml MSNs treatment for different time.

speculated that the decreasing of ROS induced by MSNs caused NF-κB activation/inactivation and further promoted the cell cycle progression and the cell proliferation. To test this hypothesis, the immunofluorescent was used to detect the nuclear translocation of NF-κB and the expression of IκB was analyzed by western blot assays. As Fig. 7A and B shown, the nuclear translocation of p50 and p65 was suppressed with the treatment of different concentration of MSNs. Western blot analysis also indicated that there was a dose-dependent increase in IκB expression in the presence of various concentrations of MSNs (Fig. 7C and D). These results indicated MSNs inhibited the activation of NF-κB.

The expression of Bcl-2, the major anti-apoptotic member of the Bcl-2 family, is under complex controls of several factors including ROS. To study the effect of MSNs on the expression of Bcl-2, western blot was carried out. As shown in Fig. 7C and D, the expression of Bcl-2 was upregulated in a dose-dependent manner with the increase of MSNs concentrations. The result indicated that MSNs upregulated the expression of Bcl-2 and activated anti-apoptotic pathway of A375 cells.

4. Discussion

Recently, a number of studies have focused on the interaction between NPs and biological systems in order to develop new strategies for design of efficient drug delivery nanocarriers. Previous studies have demonstrated that some nanocarriers can actively engage the molecular processes that are essential for regulating tumor cell functions, and further mediate tumor growth. For example, Qi et al. show there is a strong antitumor effect of chitosan NPs on human hepatoma *in vitro* and *in vivo* and the antitumor mechanism is mediated by neutralization of cell surface charge, decrease of mitochondrial membrane potential and induction of lipid peroxidation [27]. On the contrary, Zogovic et al. demonstrate that nanoC60, in contrast to its potent anticancer activity *in vitro*, can promote tumor growth *in vivo*, possibly by causing NO-dependent suppression of anticancer immune response [28]. In the present study, we showed a promotion effect of MSNs on Human Malignant Melanoma growth *in vivo* and *in vitro* (Fig. 2). Thus, the effect of NPs on tumor growth is dependent on the physicochemical properties of NPs and tumor types.

To design suitable nanocarriers for tumor treatment, it is necessary to understand the mechanism of nanocarriers-induced effects on the regulation of tumor growth. Cellular uptake of NPs is the upstream behavior of the interaction between NPs and cells. It is assumed in the literature that internalization of MSNs is partially due to their strong affinity for clathrin-coated vesicles because of their siliceous composition, unique hexagonal exterior and internal hexagonal mesopores [29]. Furthermore, it has previously been observed that MSNs are able to escape endolysosomal entrapment and then enter the cytoplasm [17]. This behavior can be attributed to the so-called “Proton Sponge” effect which is important in endosome escape [30]. From Fig. 5, we knew that MSNs were internalized in A375 cells by clathrin-mediated pathway and were transported into the cytoplasm in line with the Proton Sponge

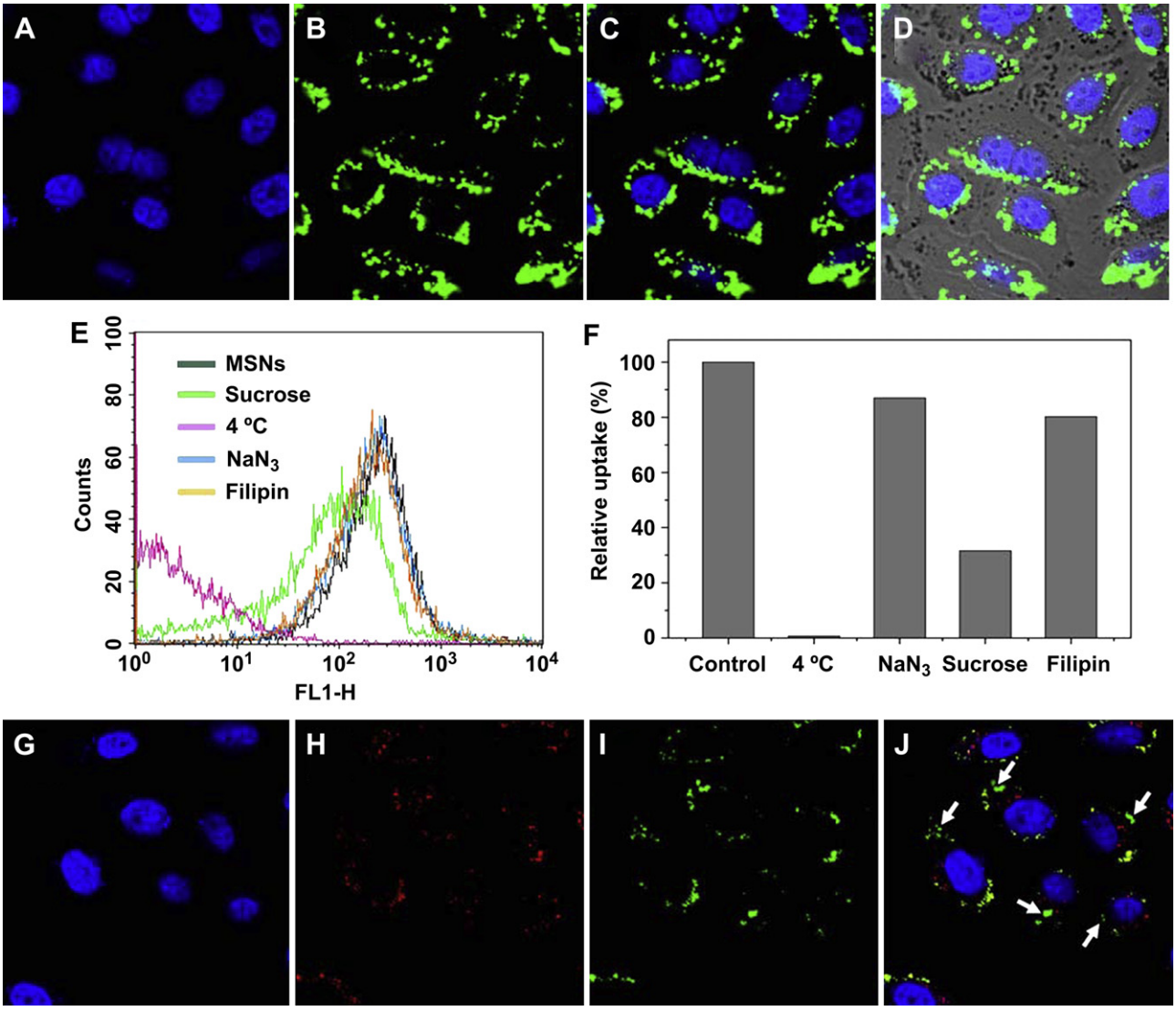

Fig. 5. Cellular uptake, uptake mechanism and intracellular localization of MSNs in A375 cells. (A–D) Confocal microscopy images of A375 cells after incubation with 50 μg/ml MSNs-FITC at 37 °C for 4 h. (A) is the DAPI fluorescence staining of cell nucleus, (B) is the MSN-FITC fluorescence image, (C) is the image of MSN-FITC fluorescence superimposed on the nucleus and (D) is the merged image of nucleus, MSNs-FITC and cells. (E, F) Quantitative analysis of cellular uptake of MSNs in cells with different inhibitor treatment: (E) Fluorescent intensity of MSNs in cells analyzed by FACS, (F) percentage of cellular uptake of MSNs. (G–J) Intracellular localization of MSNs: (G) image of cell nucleus, (H) the lysosomal compartment was stained with the LysoTracker Red probe, (I) image of MSN-FITC, and (J) the merged image of nucleus, lysosome and MSNs-FITC in cells, the arrows indicated MSNs-FITC dispersed into the cytoplasm.

effect. Moreover, it has been reported in the literature that clathrin-mediated endocytosis is dependent on NOX mediated ROS production [31]. As Fig. 6 shown, there was a clear reduction in the NOX4 expression of cells which indicating that cellular uptake of MSNs could cause the decrease of endogenous ROS level in A375 cells.

Oxidative stress is shown to be some of the key mechanisms in cellular defense after particle uptake. Many previous reports have demonstrated that the antitumor effect of the chemotherapeutic drugs loaded in NPs is mediated by elevated intracellular ROS levels, which is associated with the induction of apoptotic and necrotic cell death. These therapeutic strategies have made progress on tumor therapy, but the potential toxicity of NPs itself is also desirable to be concerned. Many studies have found that some NPs itself also induced the generation of ROS and further caused cytotoxicity, such as TiO_2, silver, silica, cerium oxide and quantum dots (QDs). On the contrary, some NPs such as the fullerene and their derivatives NPs possess a unique capacity for scavenging ROS and have been categorized as a radical sponge because it can react with free radicals. Thus, NPs can cause the increasing or decreasing of intracellular ROS by disturbing the balance between the oxidant and antioxidant processes. In this study, well-ordered MSNs specifically decreased the endogenous oxidative stress in A375 cells, but did not affect the level of ROS in HEK293T, HMEC and MDA-MB-231 cells (Fig. 3). Generally, tumor cells are under a higher level of ROS than normal cells in a normal physiology [32] and thus have a larger room to be disturbed the balance between the oxidant and antioxidant processes. According to our research, we found that there was an obviously higher level of ROS in A375 cells than HEK293T, HMEC and MDA-MB-231 cells (data not shown). This may be the possible reason of the decreasing of ROS in A375 cells induced by MSNs specifically. Understanding of mechanisms of the decrease of endogenous ROS level in A375 cells induced MSNs is of importance in order to elucidate MSNs' possible hazards and their potentials for drug/gene delivery. Previous reports have indicated that ROS are generated not only at the silica

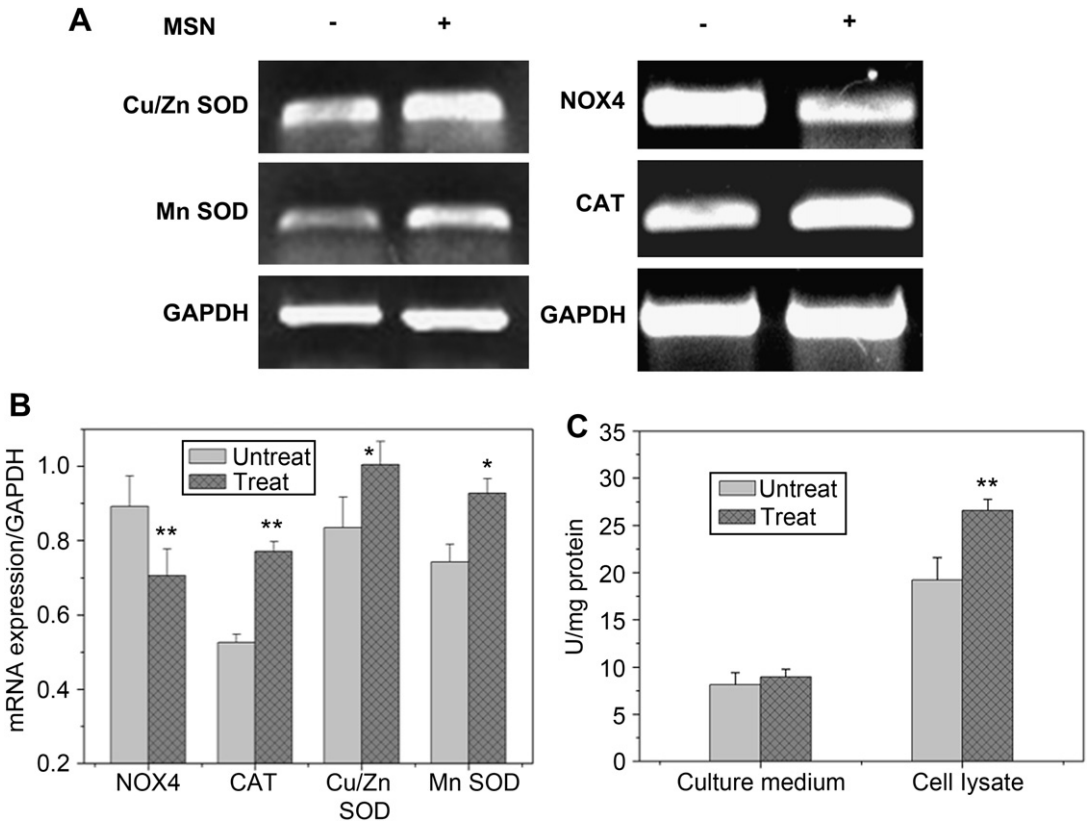

Fig. 6. Quantitative analysis of the activity/expression of CAT, SOD and NOX4 in A375 cells. (A) Reverse transcription-PCR analysis of mRNA expression of Cu/Zn SOD, Mn SOD, NOX4, and CAT. (B) is the quantitative analysis of (A). (C) CAT activity was determined with a catalase analysis kit. (Data are the means ± SD from three separate experiments. *or ** denotes statistical significance for the comparison of the mRNA level of cells treatment with or without MSNs, $^{*}p < 0.05$, $^{**}p < 0.01$).

particle surface, but also by the cells attempting to digest the silica particle. For example, some signal pathways are involved in the generation of oxidants by crystalline silica particles or by silica-activated cells. MSNs can induce MAPK/ERK kinase (MEK) and extracellular signal-regulated kinase (ERK) phosphorylation, increase inflammatory cytokines (e.g., tumor necrosis factor [TNF-α], interleukin-1 [IL-1]) expression, and activate specific transcription factors (e.g., NF-κB, AP-1) [33]. Thus, there are two possible reasons to explain the decrease of ROS in A375 cells induced by MSNs: one is that MSNs scavenge ROS through electron–electron polarization, forming a semicharge transfer complex with free radicals; the other is that MSNs lead to the activation of cell signaling pathways. According to the previous report method [34], an electron spin resonance (ESR) spectroscopy assay using the spin-trapping technique was performed to study the scavenging activity of MSNs. However, we did not find MSNs possessed scavenging free radicals activity (data not shown), which also indicating the difference of crystalline silica particles and MSNs in the structures and properties. Therefore, the reason for the scavenging of ROS in A375 cells is potentially related to the activation of cell signal pathway. In the present study, we found that upregulation of Bcl-2 was in a dose-dependent manner after the stimulus of MSNs (Fig. 7). Bcl-2-overexpressing cells have been shown to express relatively high levels of antioxidant enzymes and GSH, which indicating that Bcl-2 can upregulate the expression of antioxidant enzymes and GSH [16]. Endogenous antioxidant enzymes, such as SOD, CAT, and glutathione peroxidase function, play an important role in the balance of oxidative stress and thus protect cells from oxidative damage. Thus, it was indicated from Fig. 6 that the decrease of endogenous ROS was mainly caused by the increase of these enzymes expression and GSH level.

Bcl-2 family protein regulates apoptosis by controlling the release of mitochondrial cytochrome c via the Bax/Bak channel [35]. The expression of Bcl-2, a major anti-apoptotic member of the Bcl-2 family, is under complex controls of several factors including ROS. The anti-apoptotic function induced by MSNs was not found in our previous study [17]. A possible explanation for this behavior is that apoptotic percentage is low in untreated A375 cells. In addition, regulating Bcl-2 expression is an important element in promoting cellular survival. It has been reported that Bcl-2 family protein can promote cell survival [36]. As Fig. 3 shown, the cell cycle (S- and M-phase) and cell proliferation of A375 cells were evidently both increased after the treatment of MSNs. Therefore, it can be speculated that MSNs can affect cell proliferation by the regulating of Bcl-2 expression.

In addition, the Bcl-2 is mediated by antioxidative mechanisms that involve constitutive induction of NF-κB and subsequent upregulation of antioxidative genes [37]. In most cell types, NF-κB is typically a heterodimeric complex composed of Rel family proteins p50 and p65. It usually resides in the cytoplasm by their interaction with inhibitor of κB (IκB) proteins, and therefore remains inactive. A number of extracellular signals, such as oxidative stress, can lead to

Table 1
Determination of intracellular GSH, GSSG and GSH/GSSG level of A375 cells untreated or treated with MSNs.

MSNs	GSH (mM)	GSSG(mM)	GSH/GSSG
–	11.18 ± 0.80	1.79 ± 0.09	6.25 ± 0.76
+	13.67 ± 0.78*	0.57 ± 0.01*	23.97 ± 0.88**

Data are the means ± SD from three separate experiments. *or ** denotes statistical significance for the comparison of GSH, GSSG and GSH/GSSG level of A375 cells treated with or without MSNs, $^{*}p < 0.05$, $^{**}p < 0.01$.

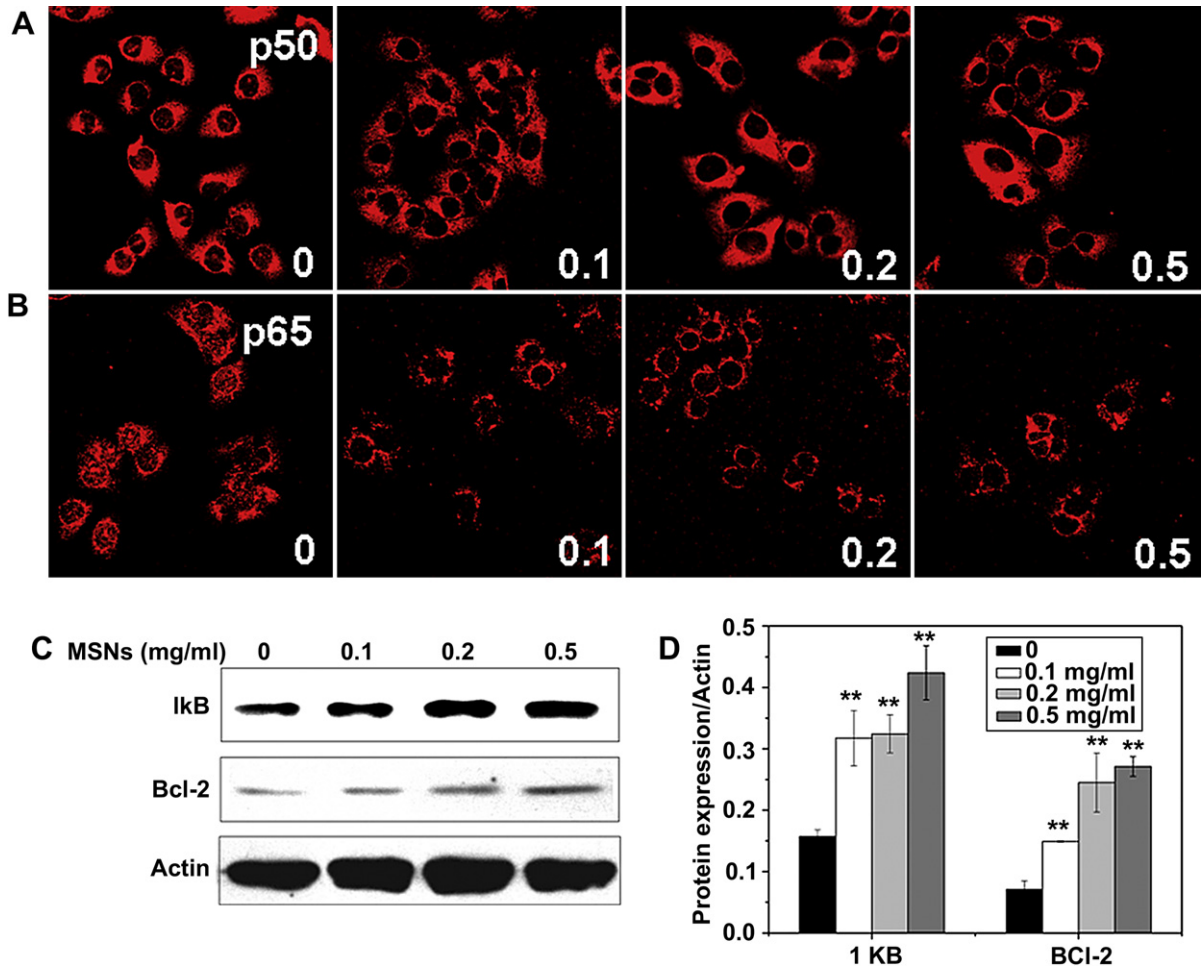

Fig. 7. Effect of MSNs on NF-κB activation and Bcl-2 expression. Confocal microscopy images of the nuclear translocation of (A) NF-κB p50 and (B) NF-κB p65 were observed in A375 cells untreated or treated with different concentration of MSNs. Western blot (C) and histogram (D) analysis of the protein expression of IκB and Bcl-2 in A375 cells untreated or treated with different concentration of MSNs. (Data are the means ± SD from three separate experiments. ** denotes statistical significance for the comparison of protein expression of cells treatment with or without MSNs, $^{**}p < 0.01$).

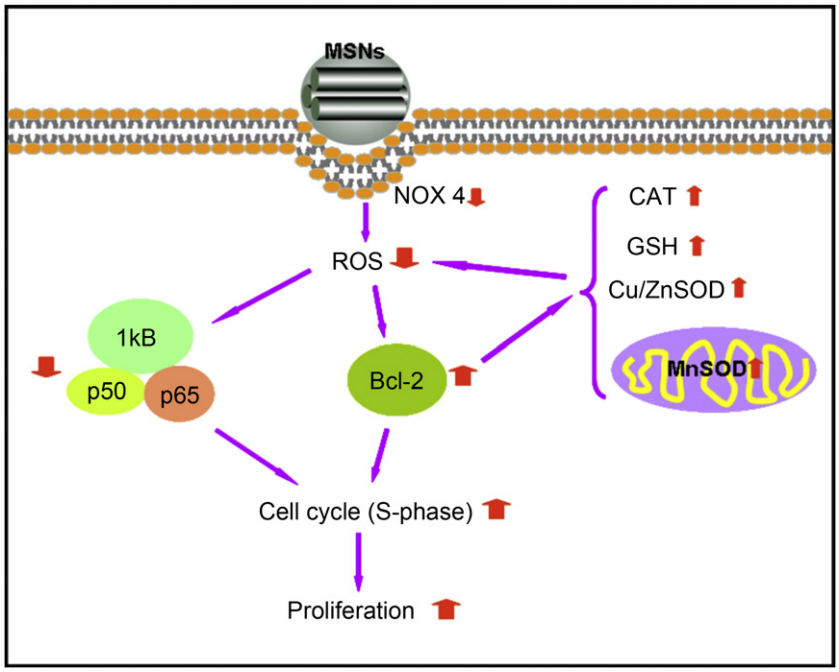

Fig. 8. Illustration of a proposal pathway of the promotion effect of MSNs on cell proliferation of A375 cells.

NF-κB activation through the phosphorylation and degradation of IκB. NF-κB complexes are in turn freed to translocate to the nucleus, where they interact with specific DNA binding sites and regulate the transcription of target genes. Among the various NF-κB target genes are many anti-apoptotic and also several proapoptotic proteins. Manna et al. demonstrate that single-walled carbon nanotube (SWCNT) cause increased oxidative stress and inhibition of cell proliferation due to the NF-κB activation by stress-related kinases activation in keratinocytes [38]. Consistent with the expression of anti-apoptotic Bcl-2 protein, the anti-apoptotic effect of NF-κB is also not observed as a result of the low apoptotic percentage in untreated A375 cells. However, there has been increasing evidence supporting that the redox-sensitive NF-κB regulates the activity and/or expression of anti-apoptotic target genes and promotes cell survival against oxidative cell death. In this study, MSNs inhibited the activation of NF-κB (Fig. 7), and thus was speculated an important reason to promote the cell cycle (S- and M-phase) and cell proliferation of A375 cells.

To the best of our knowledge, this is the first report that MSNs can promote cell proliferation of tumor cells by diminishing endogenous ROS. Unlike the upregulation of ROS level in cells, some inhibitors can be used to investigate the relationship of upstream and downstream in redox-sensitive signal pathway. For this reason, it is difficult to define the relationship of upstream and downstream involved signal molecules of our studies. Thus, the detailed mechanisms of these phenomena need to be further investigated. From the above results and the reports, we would like to propose a possible model for the MSNs regulation of cell proliferation in the redox-sensitive signal pathway (Fig. 8). During the internalization of MSNs by clathrin-mediated endocytosis, the reduction of endogenous ROS levels is caused by downregulation of NOX4 gene expression. Then the anti-apoptotic Bcl-2 expression is upregulated, which induce the elevation of endogenous antioxidant enzymes (CAT and SOD) and GSH and further to decrease the endogenous ROS levels. Moreover, the reduction of ROS inhibits the nuclear translocation of NF-κB. The upregulation of Bcl-2 expression and the inhibition of NF-κB activation can finally increase the S-phase of cell cycle and promote the cell proliferation in A375 cells.

5. Conclusions

This study shows a detailed molecular mechanism for MSNs-induced promotion of human malignant melanoma growth *in vivo* and *in vitro*. In conclusion, MSNs specifically show a promotion effect on A375 cells proliferation through an oxidative mechanism leading to the inhibition of NF-κB activation and upregulation of Bcl-2 expression. Future experiments are needed to see if it is possible to consider MSNs as antioxidant carriers to protect cell from oxidative injury. Our results indicated that MSNs as drug carriers are not necessarily suitable for all tumor treatment, which indicating the need for future investigations into the toxicity of NPs in different cell lines and animal models. Given our findings, it is necessary to investigate the detailed mechanism of tumor biological behavior induced by nanocarriers when a new kind of nanocarrier is developed and thus a more comprehensive survey of biosafety concerns about nanomedicine is recommended.

Acknowledgements

The authors acknowledge financial support from the National Hi-Technology Research and Development Program ("863" Program) (2007AA021802, 2007AA021803 and 2009AA03z322), the National Natural Science Foundation (No. 60736001 and 30900349).

Appendix. Supplementary data

Supplemental Fig. S1: Effect of MSNs on cell proliferation of different cells (A, C, E) after the incubation for 24 h with different concentration of particles, and (B, D, F) after the incubation for different time with 0.2 mg/ml particles.

Supplemental Fig. S2: Effect of MSNs on endogenous ROS level of different cells by FACS analysis.

Supplementary data associated with this article can be found in the online version of this paper at doi:10.1016/j.biomaterials.2010.04.055.

Appendix

Figures with essential color discrimination. Figs. 2–5, 7 and 8 of this article have parts that are difficult to interpret in black and white. Images in full color can be found in the online version at doi:10.1016/j.biomaterials.2010.04.055.

References

[1] Xia T, Kovochich M, Brant J, Hotze M, Sempf J, Oberley T, et al. Comparison of the abilities of ambient and manufactured nanoparticles to induce cellular toxicity according to an oxidative stress paradigm. Nano Lett 2006;6(8):1794–807.
[2] AshaRani PV, Low Kah Mun G, Hande MP, Valiyaveettil S. Cytotoxicity and genotoxicity of silver nanoparticles in human cells. ACS Nano 2009;3(2):279–90.
[3] Pan Y, Leifert A, Ruau D, Neuss S, Bornemann J, Schmid G, et al. Gold nanoparticles of diameter 1.4 nm trigger necrosis by oxidative stress and mitochondrial damage. Small 2009;5(18):2067–76.
[4] Zhang L, Laug L, Munchgesang W, Pippel E, Gosele U, Brandsch M, et al. Reducing stress on cells with apoferritin-encapsulated platinum nanoparticles. Nano Lett 2010;10(1):219–23.
[5] Huang DM, Hsiao JK, Chen YC, Chien LY, Yao M, Chen YK, et al. The promotion of human mesenchymal stem cell proliferation by superparamagnetic iron oxide nanoparticles. Biomaterials 2009;30(22):3645–51.
[6] Park JH, Gu L, von Maltzahn G, Ruoslahti E, Bhatia SN, Sailor MJ. Biodegradable luminescent porous silicon nanoparticles for in vivo applications. Nat Mater 2009;8(4):331–6.
[7] Slowing II, Vivero-Escoto JL, Wu CW, Lin VS. Mesoporous silica nanoparticles as controlled release drug delivery and gene transfection carriers. Adv Drug Deliv Rev 2008;60(11):1278–88.
[8] Slowing II, Trewyn BG, Lin VS. Mesoporous silica nanoparticles for intracellular delivery of membrane-impermeable proteins. J Am Chem Soc 2007;129(28):8845–9.
[9] Kim J, Kim HS, Lee N, Kim T, Kim H, Yu T, et al. Multifunctional uniform nanoparticles composed of a magnetite nanocrystal core and a mesoporous silica shell for magnetic resonance and fluorescence imaging and for drug delivery. Angew Chem Int Ed Engl 2008;47(44):8438–41.
[10] Slowing I, Trewyn BG, Lin VS. Effect of surface functionalization of MCM-41-type mesoporous silica nanoparticles on the endocytosis by human cancer cells. J Am Chem Soc 2006;128(46):14792–3.
[11] Qian J, Gharibi A, He S. Colloidal mesoporous silica nanoparticles with protoporphyrin IX encapsulated for photodynamic therapy. J Biomed Opt 2009;14(1):014012.
[12] Lu J, Liong M, Zink JI, Tamanoi F. Mesoporous silica nanoparticles as a delivery system for hydrophobic anticancer drugs. Small 2007;3(8):1341–6.
[13] Li Y, Rory Goodwin C, Sang Y, Rosen EM, Laterra J, Xia S. Camptothecin and Fas receptor agonists synergistically induce medulloblastoma cell death: ROS-dependent mechanisms. Anticancer Drugs 2009;20(9):770–8.
[14] Lin X, Li Q, Wang YJ, Ju YW, Chi ZQ, Wang MW, et al. Morphine inhibits doxorubicin-induced reactive oxygen species generation and nuclear factor kappaB transcriptional activation in neuroblastoma SH-SY5Y cells. Biochem J 2007;406(2):215–21.
[15] Yang J, Li H, Chen YY, Wang XJ, Shi GY, Hu QS, et al. Anthraquinones sensitize tumor cells to arsenic cytotoxicity in vitro and in vivo via reactive oxygen species-mediated dual regulation of apoptosis. Free Radic Biol Med 2004;37(12):2027–41.
[16] Jang JH, Surh YJ. Potentiation of cellular antioxidant capacity by Bcl-2: implications for its antiapoptotic function. Biochem Pharmacol 2003;66(8):1371–9.
[17] Huang X, Teng X, Chen D, Tang F, He J. The effect of the shape of mesoporous silica nanoparticles on cellular uptake and cell function. Biomaterials 2010;31(3):438–48.
[18] Abu Lila AS, Kizuki S, Doi Y, Suzuki T, Ishida T, Kiwada H. Oxaliplatin encapsulated in PEG-coated cationic liposomes induces significant tumor growth

suppression via a dual-targeting approach in a murine solid tumor model. J Control Release 2009;137(1):8–14.
[19] Faklaris O, Joshi V, Irinopoulou T, Tauc P, Sennour M, Girard H, et al. Photoluminescent diamond nanoparticles for cell labeling: study of the uptake mechanism in mammalian cells. ACS Nano 2009;3(12):3955–62.
[20] Foucaud L, Wilson MR, Brown DM, Stone V. Measurement of reactive species production by nanoparticles prepared in biologically relevant media. Toxicol Lett 2007;174(1–3):1–9.
[21] He Z, Sun X, Mei G, Yu S, Li N. Nonclassical secretion of human catalase on the surface of CHO cells is more efficient than classical secretion. Cell Biol Int 2008;32(4):367–73.
[22] Zhu MT, Feng WY, Wang B, Wang TC, Gu YQ, Wang M, et al. Comparative study of pulmonary responses to nano- and submicron-sized ferric oxide in rats. Toxicology 2008;247(2–3):102–11.
[23] Kuo JH, Jan MS, Lin YL. Interactions between U-937 human macrophages and poly(propyleneimine) dendrimers. J Control Release 2007;120(1–2):51–9.
[24] Brown DI, Griendling KK. Nox proteins in signal transduction. Free Radic Biol Med 2009;47(9):1239–53.
[25] Miao L, St Clair DK. Regulation of superoxide dismutase genes: implications in disease. Free Radic Biol Med 2009;47(4):344–56.
[26] Baeuerle PA. IkappaB-NF-kappaB structures: at the interface of inflammation control. Cell 1998;95(6):729–31.
[27] Qi L, Xu Z, Chen M. In vitro and in vivo suppression of hepatocellular carcinoma growth by chitosan nanoparticles. Eur J Cancer 2007;43(1):184–93.
[28] Zogovic NS, Nikolic NS, Vranjes-Djuric SD, Harhaji LM, Vucicevic LM, Janjetovic KD, et al. Opposite effects of nanocrystalline fullerene (C(60)) on tumour cell growth in vitro and in vivo and a possible role of immunosuppression in the cancer-promoting activity of C(60). Biomaterials 2009;30(36):6940–6.
[29] Huang DM, Hung Y, Ko BS, Hsu SC, Chen WH, Chien CL, et al. Highly efficient cellular labeling of mesoporous nanoparticles in human mesenchymal stem cells: implication for stem cell tracking. FASEB J 2005;19(14):2014–6.
[30] Boussif O, Lezoualc'h F, Zanta MA, Mergny MD, Scherman D, Demeneix B, et al. A versatile vector for gene and oligonucleotide transfer into cells in culture and in vivo: polyethylenimine. Proc Natl Acad Sci U S A 1995;92(16):7297–301.
[31] Leborgne-Castel N, Lherminier J, Der C, Fromentin J, Houot V, Simon-Plas F. The plant defense elicitor cryptogein stimulates clathrin-mediated endocytosis correlated with reactive oxygen species production in bright yellow-2 tobacco cells. Plant Physiol 2008;146(3):1255–66.
[32] Szatrowski TP, Nathan CF. Production of large amounts of hydrogen peroxide by human tumor cells. Cancer Res 1991;51(3):794–8.
[33] Mossman BT. Introduction to serial reviews on the role of reactive oxygen and nitrogen species (ROS/RNS) in lung injury and diseases. Free Radic Biol Med 2003;34(9):1115–6.
[34] Fenoglio I, Tomatis M, Lison D, Muller J, Fonseca A, Nagy JB, et al. Reactivity of carbon nanotubes: free radical generation or scavenging activity? Free Radic Biol Med 2006;40(7):1227–33.
[35] Autret A, Martin SJ. Emerging role for members of the Bcl-2 family in mitochondrial morphogenesis. Mol Cell 2009;36(3):355–63.
[36] Naoi M, Maruyama W, Yi H, Inaba K, Akao Y, Shamoto-Nagai M. Mitochondria in neurodegenerative disorders: regulation of the redox state and death signaling leading to neuronal death and survival. J Neural Transm 2009;116(11):1371–81.
[37] Fan Y, Dutta J, Gupta N, Fan G, Gelinas C. Regulation of programmed cell death by NF-kappaB and its role in tumorigenesis and therapy. Adv Exp Med Biol 2008;615:223–50.
[38] Manna SK, Sarkar S, Barr J, Wise K, Barrera EV, Jejelowo O, et al. Single-walled carbon nanotube induces oxidative stress and activates nuclear transcription factor-kappaB in human keratinocytes. Nano Lett 2005;5(9):1676–84.